Research Square

Preprints are preliminary reports that have not undergone peer review.
They should not be considered conclusive, used to inform clinical practice,
or referenced by the media as validated information.

Sinking Cities: Latent Flood Risk in Africa's Coastal Megacities

Oluwaseyi A. Dasho
seyidasho@vt.edu
Virginia Tech
Manoochehr Shirzaei
Virginia Tech
Leonard O. Ohenhen
University of California
Sonam Futi Sherpa
University of Utah
Rafael Almar
Laboratoire d'Etudes en Géophysique et Océanographie Spatiales (LEGOS)

Article

Keywords: Coastal Flooding, Vertical Land Motion, Sea Level Rise, InSAR, Africa, Flood Risk Modeling, Shared Socioeconomic Pathways

Posted Date: April 2nd, 2026

DOI: https://doi.org/10.21203/rs.3.rs-7760707/v1

License: This work is licensed under a Creative Commons Attribution 4.0 International License. Read Full License

Additional Declarations: No competing interests reported.

Abstract

Africa’s coastal cities face a heightened flood risk from relative sea level rise (RSLR), a combined effect of sea-level rise (SLR) and localized vertical land motion (VLM). However, observations of VLM remain critically scarce across Africa. Here, we present the first comprehensive, high-resolution estimate of VLM for 20 major African coastal cities (home to over 90 million people), derived from an analysis of Sentinel-1 radar datasets. We find widespread, spatially variable subsidence with median rates reaching 6.0 mm yr⁻¹ in Alexandria and 5.0 mm yr⁻¹ in Lagos, several times faster than natural background processes such as glacial isostatic adjustment, and well above the assumptions used in IPCC projections. Revising IPCC AR6 sea-level projections using up-to-date VLM increases RSLR and flood exposure substantially. For instance, in Alexandria, refined SSP2-4.5 projections raise RSL by 35.8% and the flood-exposed area by ~ 15% by 2050. Across the 20 cities, an extreme sea-level event could expose > 7 million people, > 1 million buildings and ~ USD 180 billion in assets by mid-century. Our results reveal a latent vulnerability masked by globally averaged models and demonstrate a scalable, transferable framework for risk assessment in data-scarce regions of the Global South, providing decision-ready evidence for adaptation and resilience planning.

Main

Coastal communities worldwide face an escalating threat from sea-level rise (SLR) and intensified extreme weather events driven by climate change[1,2]. Projections under various Shared Socioeconomic Pathways (SSPs) suggest that global mean SLR could range from approximately 0.28 meters under moderate emission scenarios (SSP 2-4.5) to over 2 meters under high emission scenarios by the end of the 21st century [3,4]. While global projections are indispensable, their local applicability is limited by spatially variable localized vertical land motion (VLM)[5,6]. Local land subsidence, in particular, can dramatically amplify the effects of global sea-level rise, exacerbating coastal flooding and shoreline retreat[7–12].

This challenge is nowhere more acute than in Africa, a continent grappling with a profound environmental data gap[13–15]. With relatively very few long, continuous tide-gauge records along a vast coastline, historical RSL estimates are uncertain and non-GIA drivers such as groundwater extraction and sediment compaction are often underrepresented. This data scarcity means that global models, such as IPCC projections, which often underrepresent non-GIA subsidence drivers like groundwater extraction and sediment compaction, may dangerously underestimate flood exposure in Africa's rapidly urbanizing coastal zones[16,17]. Recent studies highlight the accelerating threats of sea-level rise (SLR) along African coasts, some incorporating VLM through glacial isostatic

adjustment (GIA) models[18–22]; however, without accounting for localized land motion, the full extent of risk remains obscured.

The stakes are exceptionally high. Africa's coastal cities are experiencing unprecedented population growth and urbanization, often in an unplanned manner that increases vulnerability[23–29]. In West Africa, for instance, the coastal region is home to one-third of the population and generates 56% of the GDP[30]. Yet, since 1990, Sub-Saharan Africa has been the only region where flood mortality rates have risen[31], a trend projected to worsen[32]. Despite this, a continent-wide analysis explicitly accounting for localized VLM and its implications for land and population exposure has been missing.

Here, we address this critical gap by harnessing Interferometric Synthetic Aperture Radar (InSAR) to provide the first comprehensive, high-resolution assessment of localized VLM across 20 of Africa's most populous coastal cities, collectively home to over 90 million people (Fig. 1a). Considering the rising sea-level trends observed from available tide gauge records (Fig. 1b), the integration of spatially explicit land motion data with climate-driven sea-level projections reveals a latent vulnerability that was previously unaccounted for across the continent. This study not only provides a more accurate projection of flood exposure for Africa but also presents a powerful, transferable methodology for assessing risk in other data-scarce coastal regions across the Global South, offering a crucial tool for building climate resilience where it is most needed.

VLM Monitoring Across African Coastal Cities

We analyzed 4,288 Sentinel-1 SAR scenes along ascending tracks using advanced multitemporal InSAR techniques (see Methods). Line-of-sight (LOS) velocities were projected into the vertical direction under the assumption of uniform horizontal deformation. To ensure global consistency, the derived VLM rates were tied to the IGS14 reference frame using a coarse-resolution VLM model interpolated from GNSS observations. The resulting VLM estimates exhibit a precision better than 1 mm yr^{-1} for most cities (Supplementary Fig. S1) and show strong agreement with co-located GNSS stations (Supplementary Fig. S2).

Figure 2 summarizes the spatial and temporal patterns of VLM across 20 major African coastal cities. Negative values indicate subsidence, while positive values denote uplift. Our results reveal highly heterogeneous VLM patterns, with several of Africa's largest metropolitan areas subsiding at rates far exceeding GIA signals. Figure 2a presents the GIA VLM model overlaid by the median VLM rates obtained from InSAR at the geographic locations of each city. The GIA model indicates an uplift rate of ~ 1 mm/yr along the

eastern and southern parts of Africa. The median InSAR VLM rates across the cities range from ~-6.5 mm/yr in Alexandria to ~ 0.5 mm/yr in Mombasa, Maputo, and Durban.

The spatial distribution of VLM rates in each city, shown in individual sub-panels (Fig. 2b-2u), indicates a heterogeneous rate affecting most of the cities studied. While most cities are dominated by mild subsidence rates, Alexandria and Lagos, the two most populous cities, indicate widespread faster subsidence rates, greater than 40% of total VLM pixels (Supplementary Fig. S3). While a definitive, quantitative correlation is challenging due to the scarcity of granular ground-based data, the spatial patterns of subsidence in these hotspots strongly point to anthropogenic drivers well-documented in other global cities[12,33–35]. Alexandria exhibits widespread subsidence exceeding 6 mm yr⁻¹, particularly inland (Fig. 2f), likely driven by compaction of Nile Delta sediments exacerbated by sediment starvation following the Aswan High Dam[36,37], combined with groundwater extraction. Lagos exhibits strong spatial variability (Fig. 2q), central districts remain relatively stable, while rapidly urbanizing eastern and western peripheries experience accelerated subsidence, consistent with unregulated groundwater withdrawal, construction loading on unconsolidated alluvial sediment, and settlement of reclaimed lands[38].

Other cities, including Accra, Casablanca, Dakar, Tunis, and Tripoli, exhibit mixed patterns of mild subsidence and localized uplift, while Durban, Maputo, and Mombasa show net uplift, likely linked to regional tectonics and mantle dynamics associated with the African Superswell [39,40].

A comparison with IPCC AR6 VLM values (Fig. 2v) highlights the limitations of the global model estimate. While median InSAR rates broadly align with IPCC values, significant underestimation occurs in rapidly subsiding cities such as Alexandria (by 6.3 mm yr⁻¹) and Lagos (by 5.2 mm yr⁻¹). Moreover, the pronounced spatial variability captured by InSAR is absent in IPCC estimates, which assume uniform VLM across each site.

Relative Sea-Level Rise Projections

To refine relative sea-level (RSL) projections, we integrated our InSAR-derived VLM estimates into the IPCC AR6 No-VLM sea-level projections under three scenarios, namely, SSP1-2.6 (low emissions), SSP2-4.5 (intermediate), and SSP3-7.0 (high emissions). Figure 3 compares these refined projections with IPCC estimates at six tide-gauge stations: Tema (Accra), Alexandria, Granger Bay (Cape Town), Dakar, Durban, and Mombasa.

Across all stations and scenarios, refined projections are consistently higher than IPCC values, with the largest discrepancies at Dakar 2 (67.96%, 51.17%, and 38.06% higher for

SSP1-2.6, SSP2-4.5, and SSP3-7.0, respectively) and Alexandria (49.6%, 35.83%, and 28.33% higher). Even at the most stable site, Mombasa II, refined projections exceed IPCC estimates by 6.73%, 5.21%, and 3.81% across the scenarios. These differences widen over time, reflecting the cumulative effect of subsidence on RSL, particularly at stations with high VLM rates such as Dakar and Alexandria.

The relative contribution of VLM is most pronounced under low-emission scenarios (e.g., SSP1-2.6), where ocean-driven sea-level rise is smaller, amplifying the role of local subsidence. Conversely, under higher-emission scenarios (SSP3-7.0), climate-driven sea-level rise dominates, reducing the proportional impact of VLM. However, projected declines in groundwater levels due to climate change may exacerbate subsidence in some regions, further compounding future RSL rise.

Uncertainty analysis reinforces the importance of incorporating localized VLM. While IPCC projections exhibit broader uncertainty bands, our refined projections generally fall within these ranges except at Dakar 2, where SSP3-7.0 projections exceed IPCC upper bounds after 2060, indicating a substantial underestimation of future sea-level change in this region.

Flood-Exposed Area

To estimate potential land exposure to coastal flooding, we developed “undefended” scenarios that exclude existing or planned coastal defenses (e.g., levees, seawalls). Using connected component analysis to enforce hydrologic connectivity[41], we identified flood-prone areas based solely on topography and proximity to water bodies. Elevation data were derived from the Delta Digital Terrain Model (DTM) [42], and exposure was assessed under three SLR scenarios: SSP1-2.6, SSP2-4.5, and SSP3-7.0. For each scenario, we evaluated exposure at the 17th, 50th (median), and 83rd percentiles to capture uncertainty. Flood exposure was estimated for Extreme Sea Level (ESL) events (98th percentile coastal water level), reflecting the increasing frequency and severity of coastal flooding with rising seas[43–45].

Figure 4a–c illustrates spatial patterns of flood-exposed land in Alexandria, Douala, and Lagos under SSP2-4.5 for 2020 (blue), 2050 (yellow), and 2100 (red). Even in 2020, substantial areas are exposed during ESL events, with exposure expanding markedly by 2050 and 2100. Figure 4d summarizes exposed land areas across all cities under SSP2-4.5. By 2050, approximately 1,815 km² of land will be exposed during ESL events, increasing further by 2100. Lagos exhibits the highest exposure, with 981 ± 70 km² in 2020, $1,062 \pm 75$ km² in 2050, and $1,209 \pm 95$ km² in 2100, representing nearly 50% of its low-lying area (2,395 km²). Other cities with significant exposure include Douala, Alexandria, Accra, Luanda, Tunis, and Monrovia, all showing a consistent upward trend over time. Cities such

as Djibouti, Libreville, Mogadishu, and Tripoli exhibit lower absolute exposure but remain vulnerable to future SLR.

By 2100, the highest proportions of low-lying land exposed to flooding occur in Alexandria (67%), Maputo (61%), Lagos (57%), Mombasa (48%), and Monrovia (44%). Detailed projections for all scenarios (SSP1-2.6, SSP2-4.5, SSP3-7.0) and uncertainty ranges are provided in Supplementary Tables S1–S3, with additional bar charts in Supplementary Figure S4.

Refined vs. IPCC RSLR Exposure Estimates

Figure 5 compares flood-exposed land area estimates derived from refined RSLR projections (incorporating InSAR-based VLM) with those based on IPCC RSLR projections for 20 African coastal cities under SSP2-4.5 for 2020, 2050, and 2100. To perform this comparison, we prepared two refined flood exposure projections, one using a point value of the area-weighted VLM and the other using spatially varying VLM. Positive values indicate IPCC underestimation of exposure, while negative values denote overestimation relative to refined estimates.

Figure 5a shows the percentage differences between the area-weighted VLM flood exposure and the IPCC flood exposure. Across all cities, IPCC projections generally underestimate exposure, though most differences remain within ± 20%. Notable exceptions include Dakar and Djibouti, where refined estimates indicate substantially higher exposure by 2100.

Figure 5b incorporates spatially varying VLM, revealing greater inter-city variability. In 2020, cities such as Djibouti, Douala, Accra, and Dar es Salaam exhibit significant overestimation by IPCC, with Djibouti’s exposure overestimated by ~ 70%. In Luanda, overestimation grows between 2020 and 2050, reflecting temporal dynamics in land motion. Conversely, underestimation becomes pronounced in Libreville, Lagos, Dakar, Alexandria, Cape Town, Casablanca, Mogadishu, and Tripoli, with discrepancies widening toward 2100. Cities such as Mombasa, Monrovia, and Maputo show minimal differences across all years, indicating limited VLM influence on exposure.

These findings underscore the critical role of localized, high-resolution VLM data in refining RSLR-based flood exposure assessments. While global models, such as the IPCC, provide essential baselines, they cannot fully capture localized deformation processes that significantly alter exposure estimates. The observed discrepancies, ranging from severe underestimation to substantial overestimation, highlight the risk of misinformed adaptation strategies when VLM is ignored. Integrating spatially resolved InSAR-derived

VLM into coastal risk assessments is therefore essential for accurate planning and infrastructure resilience.

Flood-Exposed Population, Buildings, and Assets

Using population data, building footprints, and 2020 GDP per capita, we estimated projected exposure to coastal flooding in terms of population (in millions), buildings (in thousands), and assets (in billions of 2017 international USD) across 20 coastal cities (see Methods). Figure 6 summarizes these projections for 2020, 2050, and 2100 under the SSP2-4.5 scenario.

By 2050, an ESL event could impact over 7 million people, more than one million buildings, and approximately $180 billion in assets across all cities. Lagos emerges as the most vulnerable city in terms of population exposure, with its 7.2 million low-lying residents exposed to 2.59 million in 2020, increasing to 4.07 million by 2100. Alexandria also shows high exposure, with 1.89 million people at risk in 2020 (44% of its low-lying population), rising to 2.26 million by 2100 (52%). Other cities with significant exposure include Monrovia, Douala, Abidjan, and Dakar, with Douala experiencing the sharpest increase, from 480,115 in 2020 (21%) to 797,699 by 2100 (35%). In contrast, Mogadishu, Mombasa, and Cape Town exhibit relatively low exposure; for example, Mogadishu had only 9,136 exposed individuals in 2020 (4.5% of its low-lying population). The lowest exposure rates occur in Djibouti, Durban, and Tripoli.

Figure 6b shows building exposure, which broadly mirrors population trends but not always proportionally. Lagos again leads, with 528,079 buildings exposed in 2020, increasing to 848,203 by 2100. Alexandria and Monrovia also show high exposure, with 142,246 and 143,410 buildings, respectively, projected to be affected by 2100. Djibouti consistently records the lowest building exposure.

Figure 6c illustrates economic exposure, measured as asset value. Financial risk is greatest in cities with high population and infrastructure exposure, notably Lagos, Alexandria, and Douala. Lagos alone could face asset exposure exceeding $75 billion by 2100. Other cities, such as Luanda and Monrovia, also show steep increases in economic risk. Conversely, Djibouti, Mogadishu, and Tripoli exhibit minimal economic exposure due to their smaller populations and infrastructure bases.

Closing the Pan-African VLM Gap to Transform Coastal Risk Assessment

This study addresses a critical gap in coastal hazard science: the absence of a comprehensive, pan-African assessment of localized VLM and its integration into RSLR

projections. By harnessing high-resolution InSAR observations across 20 of Africa's most populous coastal cities, home to more than 90 million people, and coupling these spatially explicit land-motion estimates with climate-driven sea-level projections, we reveal a latent vulnerability that has been obscured by globally averaged models and sparse tide-gauge coverage. Beyond Africa, the framework demonstrated here constitutes a scalable, transferable methodology for first-order risk assessment in other data-scarce coastal regions across the Global South.

Our analysis shows that VLM in African coastal cities is highly heterogeneous, with subsidence hotspots such as Alexandria, Lagos, and Luanda exhibiting median rates of approximately -6.0, -5.0, and -3.8 mm yr^{-1} respectively, values that exceed GIA and diverge sharply from IPCC assumptions. These patterns reflect local anthropogenic pressures, including groundwater extraction, urban loading, sediment consolidation, and sediment starvation[12,34,39,46], superimposed on regional tectonic processes. Consequently, relying solely on GIA-based estimates of VLM, as done in prior studies[19–22], leads to a systematic underestimation of relative sea-level rise (RSLR) in the region. In contrast, cities such as Durban, Maputo, and Mombasa exhibit modest uplift, likely linked to mantle dynamics and the African Superswell[39,40]. This spatial variability underscores why regionally averaged VLM corrections are insufficient for city-scale risk assessments.

Integrating InSAR-derived VLM into SLR projections materially alters risk outlooks. In subsiding cities, refined projections yield higher RSL and greater flood exposure than IPCC baselines; for example, in Alexandria, refined projections under SSP2-4.5 indicate a 35.8% increase in RSL and a 15% increase in flood-exposed land by 2050. By contrast, uplift-dominated cities such as Mombasa show minimal differences. Crucially, spatially dense VLM observations capture intra-urban heterogeneity, revealing localized subsidence hotspots that disproportionately drive risk and are masked by point-based or averaged estimates. Reliance on homogeneous ground displacement, as in current IPCC projections, leads to systematic misestimation of flood exposure. Accounting for this spatial complexity is therefore essential for accurate elevation models and robust adaptation planning in rapidly urbanizing coastal zones.

The scale of projected exposure, over 7 million people, more than one million buildings, and approximately USD 180 billion in assets at risk by 2050 under SSP2-4.5, creates an urgent imperative for action. High-resolution VLM maps enable targeted, efficient adaptation, prioritizing rapidly subsiding districts for engineered defenses such as levees and seawalls, calibrating design heights to local RSLR, guiding land-use policy away from the most vulnerable zones, and leveraging nature-based solutions, including mangrove and wetland restoration, for wave attenuation and co-benefits. Because the convergence of unplanned urbanization, groundwater dependence, and data scarcity typifies many coasts

in the Global South, our workflow offers a transferable template for cities where subsidence is likely but under-measured.

While our analysis provides critical insights, several limitations should be acknowledged. Flood exposure estimates reflect “undefended” scenarios, excluding existing or planned coastal defenses; they therefore approximate a worst-case physical exposure. We assume linear VLM rates through 2100, a necessary simplification in data-scarce contexts, yet subsidence may evolve nonlinearly with changes in groundwater extraction, sediment budgets, loading, and tectonic activity. Future work should develop nonlinear VLM trajectories and assimilation frameworks that incorporate new observations as they become available. To isolate the physical hazard component, population, building stock, and asset values were held constant at 2020 levels; incorporating dynamic socioeconomic projections will be essential for capturing evolving exposure, although such projections introduce substantial uncertainty. Finally, this study employs a simplified static inundation model to estimate coastal flood exposure, acknowledging its limitations in representing dynamic flood processes such as flow inertia, drainage capacity, and the presence of flood defenses. However, in data-scarce regions like Africa, this approach remains one of the most feasible options for first-order, large-scale exposure assessments, enabling consistent and comparative analysis across multiple cities.

By closing the pan-African VLM gap and translating Earth observation into decision-ready risk metrics, this study fulfills its objective: it improves forecasts of flood exposure, exposes latent vulnerabilities masked by global models, and delivers a practical, transferable framework for data-scarce coastal regions. Incorporating spatially explicit VLM into RSLR projections is not merely a methodological enhancement; it is foundational to credible risk assessment and actionable adaptation in Africa and across the Global South.

Methods

VLM data

In this study, 4183 Sentinel-1A/B SAR images in the ascending direction were acquired and processed to observe the VLM across African coastal cities (Table S4). High-resolution time series of Line-Of-Sight (LOS) displacement were derived using the Wavelet-based InSAR time series algorithm [47–50]. Multi-looking factors of 12 (range) by 2 (azimuth) were applied to achieve a pixel size of approximately 28 × 28 meters. Sets of interferometric triplets with varying temporal baselines were produced using the Delaunay Triangulation method and dyadic down sampling to minimize phase closure error [47], resulting in thousands of interferograms. The 30-m resolution Shuttle Radar Topography Mission

(SRTM) Digital Elevation Model (DEM) [51] and precise satellite orbital information were used to correct topographic phase and flat earth effects [52].

A 2D minimum cost-flow algorithm [53] was applied to a sparse set of elite (less noisy) pixels [54] to estimate absolute phase changes. Unwrapped phase values of interferograms were combined using a reweighted least-squares approach to produce LOS time series displacement for each pixel [48]. To correct for the atmospheric delay in the SAR interferometry, 2D smoothing splines [47] and wavelet-based filters [50] were applied. LOS rates, derived from the best-fitting lines of each pixel's time series, were projected to the vertical direction, assuming horizontal displacement can be modeled using a 2D polynomial and removed.

We tied the local VLM measurements from InSAR to the IGS14 global reference frame using available GNSS VLM dataset and the global VLM model by [39], which captures large-scale VLM signals from glacial isostatic adjustment, tectonics, and water storage changes worldwide. An affine transformation was implemented to align the localized InSAR VLM dataset with the global IGS14 coordinate system[5,55], accounting for geospatial offsets and scaling differences. This integration ensured consistent cross-comparison and analysis within the broader global spatial reference frame. The Lagos VLM dataset was obtained from [56].

Coastal water level data

Coastal water level data for African coastal cities were obtained from [57]. The dataset provides coastal water levels at the 98th percentile, referred to as Extreme Sea Level (ESL). ESL results from the combination of several different coastal processes: the regional sea level anomaly due to the steric effect, ocean circulation, and transfer of mass from the continents (ice sheets, glaciers, land water) to the ocean, storm surge due to atmospheric pressure and winds, astronomical tide, and wave effects here referred to collectively as runup, which includes a time-averaged component (setup) and an oscillatory component (swash) [58]. ESL results from a combination of satellite altimetry [59], tide (FES2014) and surge models (MOG2D) [60], and wave reanalyses (ECMWF, ERAInterim) [61], taking into account the key contribution of wave runup at open coasts [62].

Elevation Data

We utilized the global coastal Digital Terrain Model (DTM), specifically DeltaDTM [42] elevation data to model flood exposure. DeltaDTM is designed to provide accurate elevation data for low-lying coastal areas, which are at risk from extreme water levels,

subsidence, and changing weather patterns. DeltaDTM offers a horizontal spatial resolution of approximately 30 meters and a vertical mean absolute error (MAE) of 0.45 meters [42]. It improves on existing elevation datasets by correcting biases in the CopernicusDEM with data from the ICESat-2 and spaceborne lidar missions such as GEDI (Global Ecosystem Dynamics Investigation). The process involves removing non-terrain cells, such as canopy and buildings, and filling gaps using spatial interpolation. This approach yields a more accurate representation of the bare earth surface, rendering DeltaDTM a valuable resource for applications such as coastal flood impact modeling and coastal management.

Sea Level Projection

We utilize regional sea-level projections data (medium confidence) from the IPCC Sixth Assessment Report (AR6) [3,63]. The AR6 projections for sea level rise incorporate a comprehensive range of geophysical factors, including contributions from ice sheets, thermal expansion, glacier melt, VLM, sterodynamic effects, and land water storage. To prevent double counting of VLM, we used the SLR projections excluding the VLM contribution in our study.

The database provides sea-level projections at both 1^{o} x 1^{o} global grid and at tide-gauge stations worldwide under five Shared Socioeconomic Pathways (SSP) scenarios: SSP1-1.9 (limiting warming to 1.5°C), SSP1-2.6 (keeping warming below 2.0°C), SSP2-4.5 (projecting 2.7°C warming), SSP3-7.0 (medium to high emissions scenario with 2.8–4.6°C warming), and SSP5-8.5 (high emissions scenario with 3.3–5.7°C warming). This study used the SSP 1-2.6, SSP 2-4.5 and SSP 3–7.0 with a particular focus on the SSP2-4.5 scenario, which represents the current emissions trajectory, using the 17th (lower bound), 50th (median), and 83rd (upper bound) percentile projections to capture uncertainties.

Population Data

The population estimates for each of the African coastal cities were derived from the WorldPop gridded population dataset [64]. The WorldPop's constrained top-down modeling approach leverages a global database containing census and projection counts based on administrative units for each year from 2000 to 2020. This data is subsequently broken down into grid cell-based counts using a collection of detailed geospatial datasets, with estimations confined to areas identified as containing built settlements.

Building Footprint Data

The property data for each African coastal city was derived from the third version of Google building footprints [65], and where those were unavailable, they were obtained from Microsoft building footprints [66]. These building footprints are composed of outlines of

buildings derived from high-resolution satellite imagery. For the Google building footprint, the confidence threshold value of 80% precision was used in this study.

Flood Exposure Model

We used the static inundation model with hydraulic connectivity [67] to compute the spatial extent of episodic flooding in 20 African coastal cities. The input data for the model includes the DeltaDTM, the VLM data, IPCC sea level rise projections, and extreme coastal water levels. To implement the model, first, the VLM rates data were sampled on the DeltaDTM (30 m resolution). Next, assuming a linear VLM rate, the elevation data was modified to account for VLM projections from the base year of the elevation data to the target years of 2020, 2050 and 2100. Subsequently, the mean coastal water level (2003–2015) and the SLR projections for 2020, 2050, and 2100 were subtracted from the modified elevation data (updated for the VLM projection). Here, we consider areas with a projected height below zero as being inundated. To remove isolated inundated grid cells (i.e., cells with no hydrological connection to a water body), connected-component analysis was implemented. The connected-component analysis reduces errors associated with the static bathtub model. Note that the model presented here does not account for any defense structure not captured in the elevation data.

To account for uncertainties in the input data, the 17th and 83rd percentiles for geocentric SLR projections, the ± 1 standard deviation of the VLM and the inherent error in the elevation data. This provides an estimate of uncertainties associated with the projections of the flood exposure.

$$Inun_{med} = DEM + (t - t_0) * VLM - (SLR_{50} + CWL)$$

$$Inun_{high} = Inun_{med} - \sqrt{{DEM_{err}}^2 + ((t - t_0) * VLM_{SD})^2 - (SLR_{83} - SLR_{50})^2}$$

$$Inun_{low} = Inun_{med} + \sqrt{{DEM_{err}}^2 + ((t - t_0) * VLM_{SD})^2 - (SLR_{50} - SLR_{17})^2}$$

where $Inun_{med}$, $Inun_{low}$ and $Inun_{high}$ represent the median, lower and upper bounds, respectively, of the models. DEMerr is the vertical accuracy of the elevation data. t represents the projection target years of 2020, 2050 and 2100. t_0 represents the base year of the elevation data. VLM_{SD} is one standard deviation of the VLM data. CWL represents the mean NCWL or ECWL. SLR_{17}, SLR_{50} and SLR_{83} represent the 17th, 50th and 83rd percentiles, respectively, from the geocentric SLR projections.

Asset Cost Estimation Approach

The exposed population was translated into asset exposure using the sub-national GDP per capita value. The GDP per capita values were obtained from a downscaled gridded global

dataset by [68], which provides GDP at Purchasing Power Parity (PPP) (in 2017 international dollars) from 1990 to 2022. For this study, we used 2020 data at the admin-2 level, with a spatial resolution of 5 arc-min (~ 10 km). Specifically, GDP per capita values were multiplied by the exposed population counts to derive total GDP within the exposed extent. These were subsequently converted to asset values by applying an assets-to-GDP ratio of 2.8, following [69]:

$$\text{Asset Cost} = 2.8 \times \text{Exposed Population} \times \text{GDP per Capita}$$

Declarations

Competing interests:

Authors declare that they have no competing interests.

Funding:

U.S. Department of Defense

Author Contribution

Conceptualization: OAD, MS; Methodology: OAD, MS, LOO, SFS, RA; Investigation: OAD, MS; Visualization: OAD, MS, LOO; Funding acquisition: MS; Project administration: OAD, MS; Supervision: MS; Writing – original draft: OAD; Writing – review & editing: OAD, MS, LOO, SFS, RA.

Acknowledgement

Acknowledgements: The OD and MS gratefully acknowledge funding support from the U.S. Department of Defense (DOD). Special thanks to Robert Kopp for his valuable guidance, and to Philip Minderhoud and Katerina Seeger for engaging and robust discussions on the work.

Data Availability

SAR data sets used in this study can be found at the Alaska satellite facilities at https://vertex.daac.asf.alaska.edu/. Lagos VLM dataset can be obtained from https://doi.org/10.7294/19738957. Tide gauge data sets are available on the PSMSL

website https://psmsl.org/data/obtaining/map.html. Google Open Buildings, 2023. URL: https://sites.research.google/open-buildings/. Microsoft. Microsoft Global ML footprints, 2023. URL: https://github.com/microsoft/GlobalMLBuildingFootprints. GDP per capita at sub-national level can be found at https://zenodo.org/records/13943886. The flood exposure data in GeoTIFF format, VLM datasets, and associated standard deviation datasets will be permanently archived in the Virginia Tech Data Repository. Currently, these datasets are temporarily available at https://data.mendeley.com/preview/x2h5xzsf8r?a=2c121731-3b12-4865-8c88-14dc598d3ee3 .

References

1. Aghakouchak, A. *et al.* Climate Extremes and Compound Hazards in a Warming World. *Annu. Rev. Earth Planet. Sci.* 48, 519–548 (2020).
2. Seneviratne, S.I., X. Zhang, M. Adnan, W. Badi, C. Dereczynski, A. Di Luca, S. Ghosh, I. Iskandar, J. Kossin, S. Lewis & F. Otto, I. Pinto, M. Satoh, S.M. Vicente-Serrano, M. Wehner, and B. Z. Weather and Climate Extreme Events in a Changing Climate. in Climate Change 2021 – The Physical Science Basis 1513–1766 (Cambridge University Press, 2021). doi:10.1017/9781009157896.013.
3. Fox-Kemper, B. et al. Ocean, Cryosphere and Sea Level Change. In Climate Change 2021: The Physical Science Basis. Contribution of WorkingGroup I to the Sixth Assessment Report of the Intergovernmental Panel on Climate Change. Climate Change 2021 – The Physical Science Basis https://www.cambridge.org/core/books/climate-change-2021-the-physical-science-basis/ocean-cryosphere-and-sea-level-change/F61263910A16BD9FDE86921E85E1E4D5 (2023).
4. Garner, A. J. *et al.* Evolution of 21st Century Sea Level Rise Projections. *Earth's Futur.* 6, 1603–1615 (2018).
5. Ohenhen, L. O., Shirzaei, M., Ojha, C. & Kirwan, M. L. Hidden vulnerability of US Atlantic coast to sea-level rise due to vertical land motion. *Nat. Commun.* 14, 2038 (2023).
6. Sherpa, S. F., Shirzaei, M. & Ojha, C. Disruptive Role of Vertical Land Motion in Future Assessments of Climate Change-Driven Sea-Level Rise and Coastal Flooding Hazards in the Chesapeake Bay. *J. Geophys. Res. Solid Earth* 128, 1–18 (2023).
7. Kopp, R. E. *et al.* Probabilistic 21st and 22nd century sea-level projections at a global network of tide-gauge sites. *Earth's Futur.* 2, 383–406 (2014).
8. Nicholls, R. J. *et al.* A global analysis of subsidence, relative sea-level change and coastal flood exposure. *Nat. Clim. Chang.* 11, 338–342 (2021).

9. Barnard, P. L. et al. Projections of multiple climate-related coastal hazards for the US Southeast Atlantic. Nat. Clim. Chang. (2024) doi:10.1038/s41558-024-02180-2.
10. Shirzaei, M. *et al.* Measuring, modelling and projecting coastal land subsidence. *Nat. Rev. Earth Environ.* 2, 40–58 (2021).
11. Avornyo, S. Y. *et al.* The contribution of coastal land subsidence to potential sea-level rise impact in data-sparse settings: The case of Ghana's Volta delta. *Quat. Sci. Adv.* 14, 100175 (2024).
12. Wu, P. C., Wei, M. & D'Hondt, S. Subsidence in Coastal Cities Throughout the World Observed by InSAR. *Geophys. Res. Lett.* 49, (2022).
13. Le Cozannet, G. *et al.* Vertical ground motion and historical sea-level records in Dakar (Senegal). *Environ. Res. Lett.* 10, (2015).
14. Woodworth, P., Aman, A. & Aarup, T. Sea level monitoring in Africa. *African J. Mar. Sci.* 29, 321–330 (2007).
15. Marcos, M. *et al.* Coastal Sea Level and Related Fields from Existing Observing Systems. *Surv. Geophys.* 40, 1293–1317 (2019).
16. Li, T. *et al.* Vertical land motion is underestimated in sea-level projections from the Oka estuary, northern Spain. *Sci. Rep.* 14, 31302 (2024).
17. Naish, T. *et al.* The Significance of Interseismic Vertical Land Movement at Convergent Plate Boundaries in Probabilistic Sea-Level Projections for AR6 Scenarios: The New Zealand Case. *Earth's Futur*. 12, (2024).
18. Nhantumbo, B. J., Nilsen, J. E. Ø., Backeberg, B. C. & Reason, C. J. C. The relationship between coastal sea level variability in South Africa and the Agulhas Current. *J. Mar. Syst.* 211, 103422 (2020).
19. Mohamed, B., Abdallah, A. M., Alam El-Din, K., Nagy, H. & Shaltout, M. Inter-Annual Variability and Trends of Sea Level and Sea Surface Temperature in the Mediterranean Sea over the Last 25 Years. *Pure Appl. Geophys.* 176, 3787–3810 (2019).
20. Kemgang Ghomsi, F. E. *et al.* Sea level variability in Gulf of Guinea from satellite altimetry. *Sci. Rep.* 14, 4759 (2024).
21. Arame, D., Bamol, A. S., Habib, B. D., Patrick, M. & Luc, D. Impact of climate variability modes on trend and interannual variability of sea level near the West African coast. *African J. Environ. Sci. Technol.* 17, 157–166 (2023).
22. Allison, L. C., Palmer, M. D. & Haigh, I. D. Projections of 21st century sea level rise for the coast of South Africa. *Environ. Res. Commun.* 4, 025001 (2022).
23. Vousdoukas, M. I. *et al.* African heritage sites threatened as sea-level rise accelerates. *Nat. Clim. Chang.* 12, 256–262 (2022).

24. Dube, K., Nhamo, G. & Chikodzi, D. Flooding trends and their impacts on coastal communities of Western Cape Province, South Africa. *GeoJournal* 87, 453–468 (2022).
25. Douglas, I. *et al.* Unjust waters: climate change, flooding and the urban poor in Africa. *Environ. Urban.* 20, 187–205 (2008).
26. Okunola, O. H. et al. Quantifying Socio-Economic and Environmental Impacts of Flood Risk and Management Strategies in Coastal Cities of Africa: A Study of Nigeria and South Africa. SSRN Electron. J. (2022) doi:10.2139/ssrn.4193705.
27. Neumann, B., Vafeidis, A. T., Zimmermann, J. & Nicholls, R. J. Future coastal population growth and exposure to sea-level rise and coastal flooding - A global assessment. *PLoS One* 10, (2015).
28. Hzami, A. *et al.* Alarming coastal vulnerability of the deltaic and sandy beaches of North Africa. *Sci. Rep.* 11, 2320 (2021).
29. Yankson, P. W. K., Owusu, A. B., Owusu, G., Boakye-Danquah, J. & Tetteh, J. D. Assessment of coastal communities' vulnerability to floods using indicator-based approach: a case study of Greater Accra Metropolitan Area, Ghana. *Nat. Hazards* 89, 661–689 (2017).
30. Croitoru, L., Miranda, J. J. & Sarraf, M. The Cost of Coastal Zone Degradation in West Africa. (World Bank, Washington, DC, 2019). doi:10.1596/31428.
31. Tanoue, M., Hirabayashi, Y. & Ikeuchi, H. Global-scale river flood vulnerability in the last 50 years. *Sci. Rep.* 6, (2016).
32. Jongman, B., Ward, P. J. & Aerts, J. C. J. H. Global exposure to river and coastal flooding: Long term trends and changes. *Glob. Environ. Chang.* 22, 823–835 (2012).
33. Buzzanga, B. *et al.* Localized uplift, widespread subsidence, and implications for sea level rise in the New York City metropolitan area. *Sci. Adv.* 9, 7–12 (2023).
34. Parsons, T., Wu, P., (Matt) Wei, M. & D'Hondt, S. The Weight of New York City: Possible Contributions to Subsidence From Anthropogenic Sources. *Earth's Futur.* 11, (2023).
35. Tay, C. *et al.* Sea-level rise from land subsidence in major coastal cities. *Nat. Sustain.* 5, 1049–1057 (2022).
36. Stanley, J.-D. & Clemente, P. L. Increased Land Subsidence and Sea-Level Rise Are Submerging Egypt's Nile Delta Coastal Margin. GSA Today 4–11 (2017) doi:10.1130/GSATG312A.1.
37. Bohannon, J. The Nile Delta's Sinking Future. *Science (80-.).* 327, 1444–1447 (2010).
38. Ikuemonisan, F. E. & Ozebo, V. C. Characterisation and mapping of land subsidence based on geodetic observations in Lagos, Nigeria. *Geod. Geodyn.* 11, 151–162 (2020).
39. Hammond, W. C., Blewitt, G., Kreemer, C. & Nerem, R. S. GPS Imaging of Global Vertical Land Motion for Studies of Sea Level Rise. *J. Geophys. Res. Solid Earth* 126,

(2021).

40. Nyblade, A. A. & Robinson, S. W. The African Superswell. *Geophys. Res. Lett.* 21, 765–768 (1994).
41. Ohenhen, L. O., Shirzaei, M., Ojha, C., Sherpa, S. F. & Nicholls, R. J. Disappearing cities on US coasts. *Nature* 627, 108–115 (2024).
42. Pronk, M. *et al.* DeltaDTM: A global coastal digital terrain model. *Sci. Data* 11, 1–18 (2024).
43. Dahl, K. A., Fitzpatrick, M. F. & Spanger-Siegfried, E. Sea level rise drives increased tidal flooding frequency at tide gauges along the U.S. East and Gulf Coasts: Projections for 2030 and 2045. *PLoS One* 12, e0170949 (2017).
44. Taherkhani, M. *et al.* Sea-level rise exponentially increases coastal flood frequency. *Sci. Rep.* 10, 1–17 (2020).
45. Vitousek, S. *et al.* Doubling of coastal flooding frequency within decades due to sea-level rise. *Sci. Rep.* 7, (2017).
46. Ikuemonisan, F. E., Ozebo, V. C. & Olatinsu, O. B. Geostatistical evaluation of spatial variability of land subsidence rates in Lagos, Nigeria. *Geod. Geodyn.* 11, 316–327 (2020).
47. Lee, J. C. & Shirzaei, M. Novel algorithms for pair and pixel selection and atmospheric error correction in multitemporal InSAR. *Remote Sens. Environ.* 286, 113447 (2023).
48. Shirzaei, M. A wavelet-based multitemporal DInSAR algorithm for monitoring ground surface motion. *IEEE Geosci. Remote Sens. Lett.* 10, 456–460 (2013).
49. Shirzaei, M., Bürgmann, R. & Fielding, E. J. Applicability of Sentinel-1 Terrain Observation by Progressive Scans multitemporal interferometry for monitoring slow ground motions in the San Francisco Bay Area. *Geophys. Res. Lett.* 44, 2733–2742 (2017).
50. Shirzaei, M. & Bürgmann, R. Topography correlated atmospheric delay correction in radar interferometry using wavelet transforms. *Geophys. Res. Lett.* 39, 1–6 (2012).
51. Farr, T. G. *et al.* The shuttle radar topography mission. *Rev. Geophys.* 45, 1–13 (2007).
52. Franceschetti, G. & Lanari, R. Synthetic aperture radar processing CRC press. Electron. Eng. Syst. Ser. (1999).
53. Mario Costantini, T. A novel phase unwrapping method based on network programming. *IEEE Trans. Geosci. Remote Sens.* 36, 813–821 (1998).
54. Costantini, M. & Rosen, P. A. Generalized phase unwrapping approach for sparse data. in International Geoscience and Remote Sensing Symposium (IGARSS) vol. 1 267–269 (1999).
55. Blackwell, E., Shirzaei, M., Ojha, C. & Werth, S. Tracking California’s sinking coast from space: Implications for relative sea-level rise. *Sci. Adv.* 6, 1–10 (2020).

56. Ohenhen, L. O. & Shirzaei, M. Land Subsidence Hazard and Building Collapse Risk in the Coastal City of Lagos, West Africa. *Earth's Futur.* 10, 1–12 (2022).
57. Almar, R. *et al.* A global analysis of extreme coastal water levels with implications for potential coastal overtopping. *Nat. Commun.* 12, 1–9 (2021).
58. Melet, A., Meyssignac, B., Almar, R. & Le Cozannet, G. Erratum to: Under-estimated wave contribution to coastal sea-level rise (Nature Climate Change, (2018), 8, 3, (234–239), 10.1038/s41558-018-0088-y). *Nat. Clim. Chang.* 8, 840 (2018).
59. Pujol, M. I. *et al.* DUACS DT2014: The new multi-mission altimeter data set reprocessed over 20 years. *Ocean Sci.* 12, 1067–1090 (2016).
60. Carrere, L., Lyard, F. H., Cancet, M. & Guillot, A. Finite Element Solution FES2014, a new tidal model – Validation results and perspectives for improvements. ESA Living Planet Conf. (2016).
61. Dee, D. P. *et al.* The ERA-Interim reanalysis: Configuration and performance of the data assimilation system. *Q. J. R. Meteorol. Soc.* 137, 553–597 (2011).
62. Stockdon, H. F., Holman, R. A., Howd, P. A. & Sallenger, A. H. Empirical parameterization of setup, swash, and runup. *Coast. Eng.* 53, 573–588 (2006).
63. Garner, G. G. et al. IPCC AR6 Sea-Level Rise Projections. https://podaac.jpl.nasa.gov/announcements/2021-08-09-Sea-level-projections-from-the-IPCC-6th-AssessmentReport. (2021).
64. Tatem, A. J. WorldPop, open data for spatial demography. *Sci. Data* 4, 170004 (2017).
65. Sirko, W. et al. Continental-Scale Building Detection from High Resolution Satellite Imagery. (2021).
66. Microsoft. Microsoft global ml footprints. https://github.com/microsoft/%0AGlobalMLBuildingFootprints (2023).
67. Kulp, S. A. & Strauss, B. H. New elevation data triple estimates of global vulnerability to sea-level rise and coastal flooding. *Nat. Commun.* 10, 4844 (2019).
68. Kummu, M., Kosonen, M. & Masoumzadeh Sayyar, S. Downscaled gridded global dataset for gross domestic product (GDP) per capita PPP over 1990–2022. *Sci. Data* 12, 178 (2025).
69. Hallegatte, S., Green, C., Nicholls, R. J. & Corfee-Morlot, J. Future flood losses in major coastal cities. *Nat. Clim. Chang.* 3, 802–806 (2013).

Figures

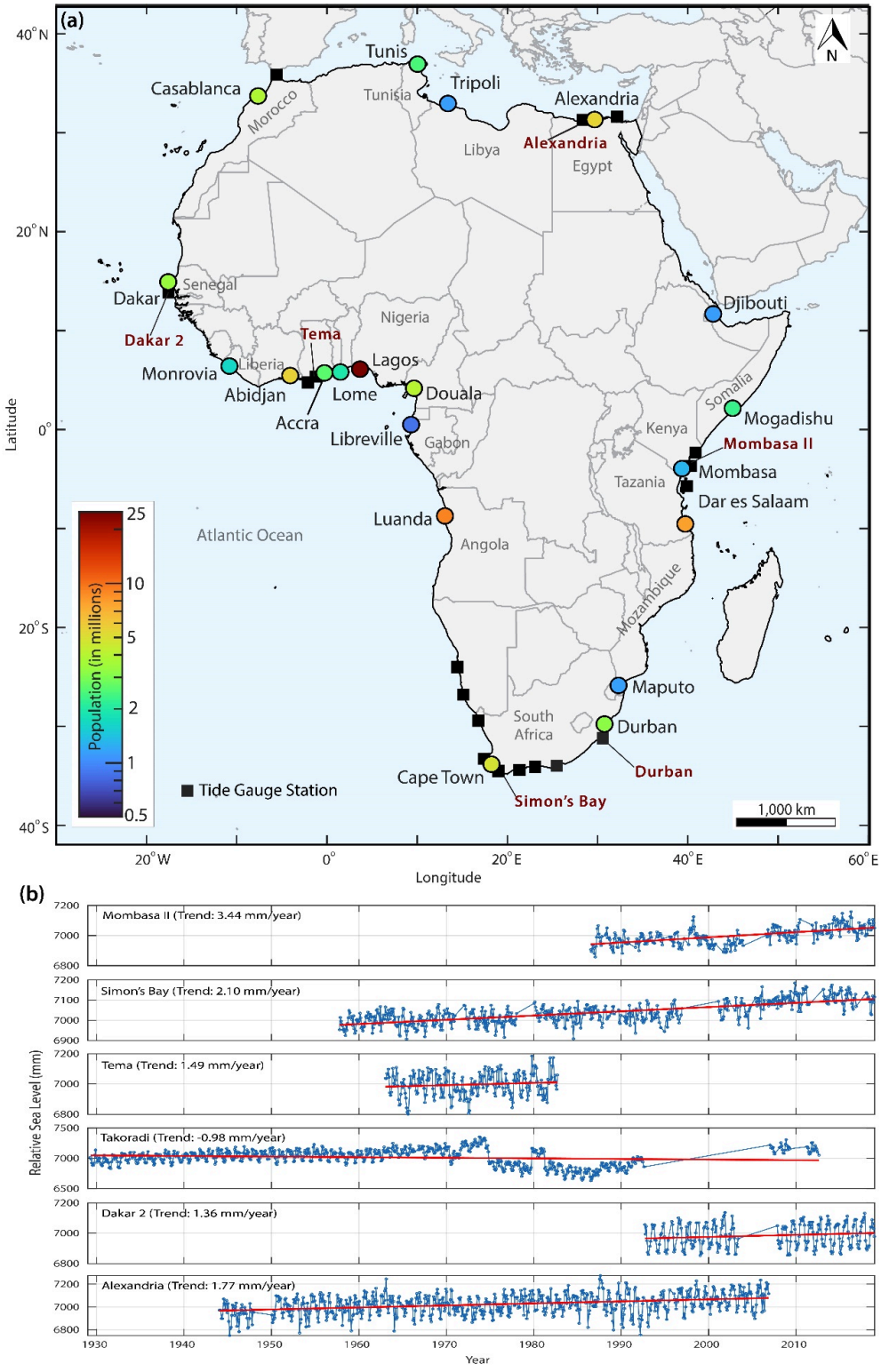


Figure 1

Coastal Cities, Tide Gauge Locations, and Relative Sea Level Trends in Africa. (a) Study area with coastal cities analyzed in this study, with color-coded markers representing the population size of each city (in millions). Tide gauge stations used in the IPCC Sea Level Rise (SLR) projections are indicated by black squares. Tide gauge stations located in cities under this study are labeled, including Dakar 2, Tema, Simon's Bay, Mombasa II,

Alexandria, and Durban. The map provides an overview of urban coastal populations and their proximity to tide gauge measurements used for long-term sea level monitoring and projections. (b) The graph shows historical relative sea level records from the six tide gauge stations located in cities under this study, spanning multiple decades. The data, sourced from the Permanent Service for Mean Sea Level (PSMSL), illustrate long-term trends in sea level at different African coastal locations.

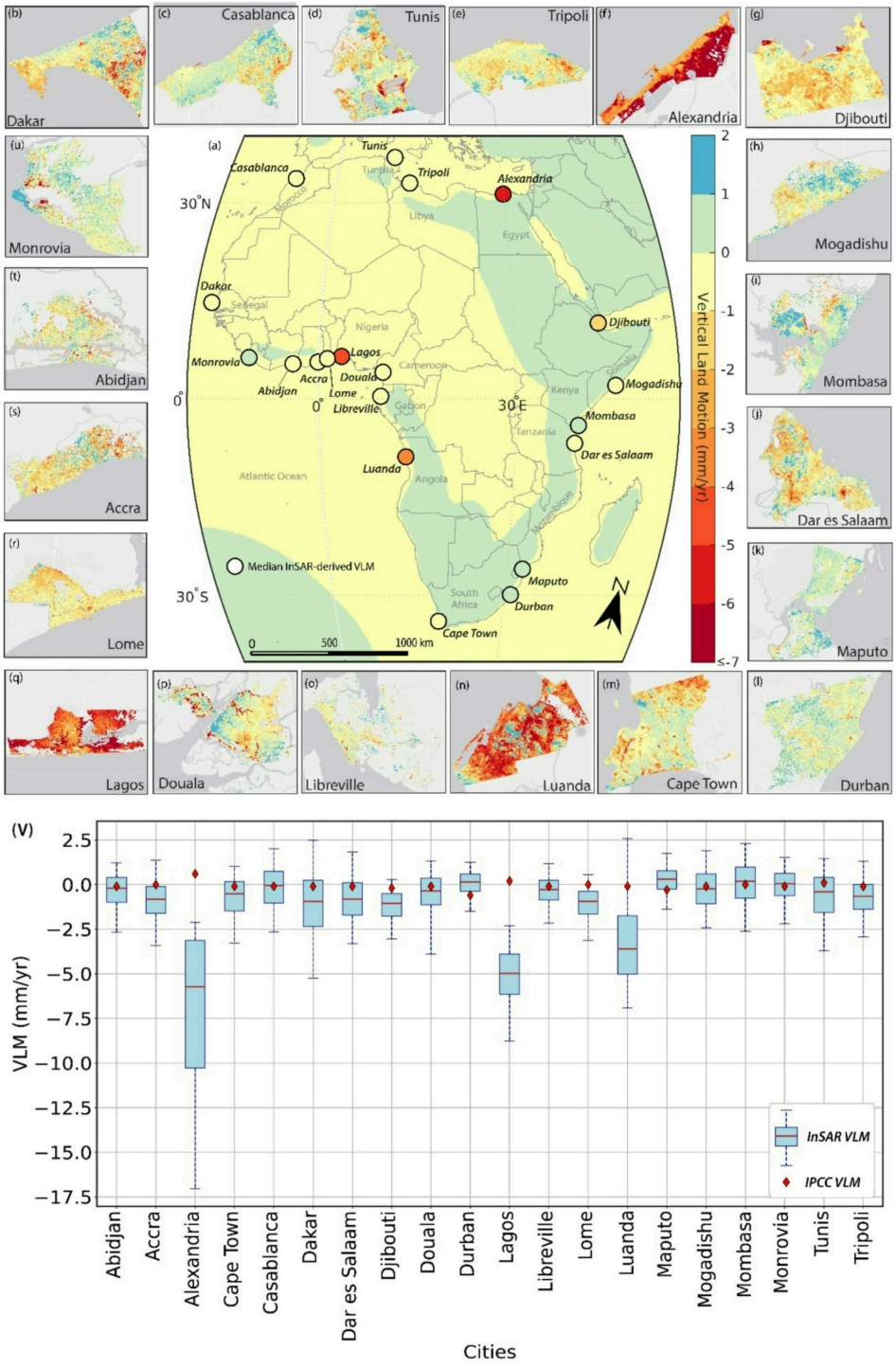


Figure 2

Vertical Land Motion (VLM) Across African Coastal Cities (a) Map of Africa displaying the median VLM for each coastal city (represented by circles) overlaid on the Glacial Isostatic Adjustment (GIA) VLM model from Peltier et al. (2015, 2018). The color scale represents VLM values in mm/year, with positive values (blue) indicating uplift and negative values (red) indicating subsidence. (b–u) Individual VLM maps for selected African coastal cities, derived from InSAR data. Each city's map illustrates localized vertical land motion patterns, with color coding consistent with the legend—blue for uplift and red for subsidence. **(v)** Box plot comparing InSAR-derived VLM values for each city. The plot represents the distribution of VLM values, showing the 5th to 95th percentile range for each city. The red diamond markers indicate the IPCC VLM values for the corresponding cities.

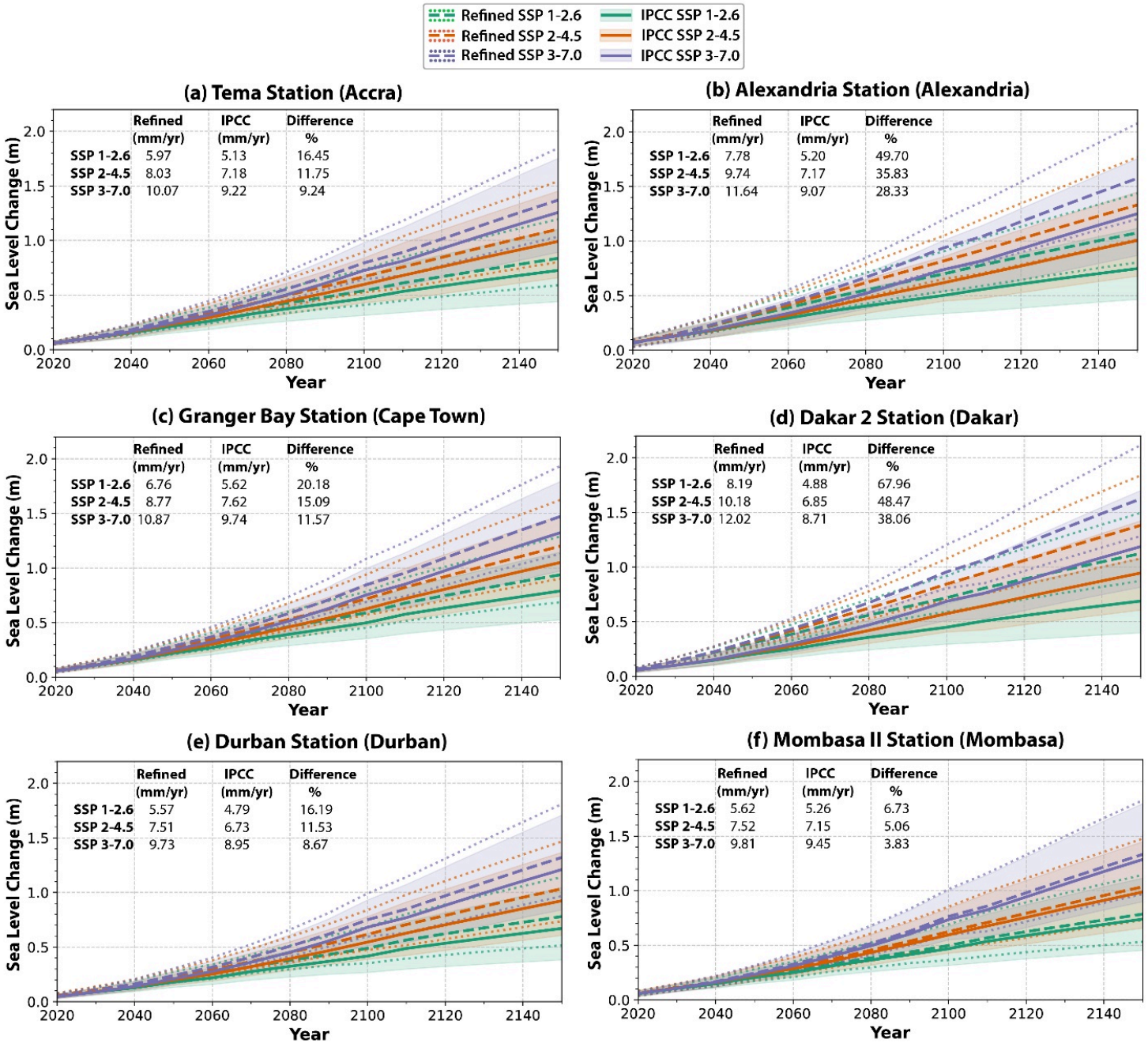


Figure 3

Projected Sea Level Change at Six Tide Gauge Stations Under Refined and IPCC Projections. The figure presents sea level rise (SLR) projections for six African coastal tide gauge stations: (a) Tema Station (Accra), (b) Alexandria Station (Alexandria), (c) Granger Bay Station (Cape Town), (d) Dakar 2 Station (Dakar), (e) Durban Station (Durban), and (f) Mombasa II Station (Mombasa). Each panel compares the refined SLR projections (dashed lines) with the IPCC SLR projections (solid lines) under three SSP scenarios: SSP1-2.6 (green), SSP2-4.5 (orange), SSP3-7.0 (blue). The shaded regions represent uncertainty bounds for each scenario. The tables in each panel provide SLR rates (mm/yr) for both refined and IPCC projections along with the percentage difference between them. The results highlight significant variations in sea level change projections across locations, with some cities, such as Alexandria and Dakar, showing considerable underestimation in the original IPCC projections.

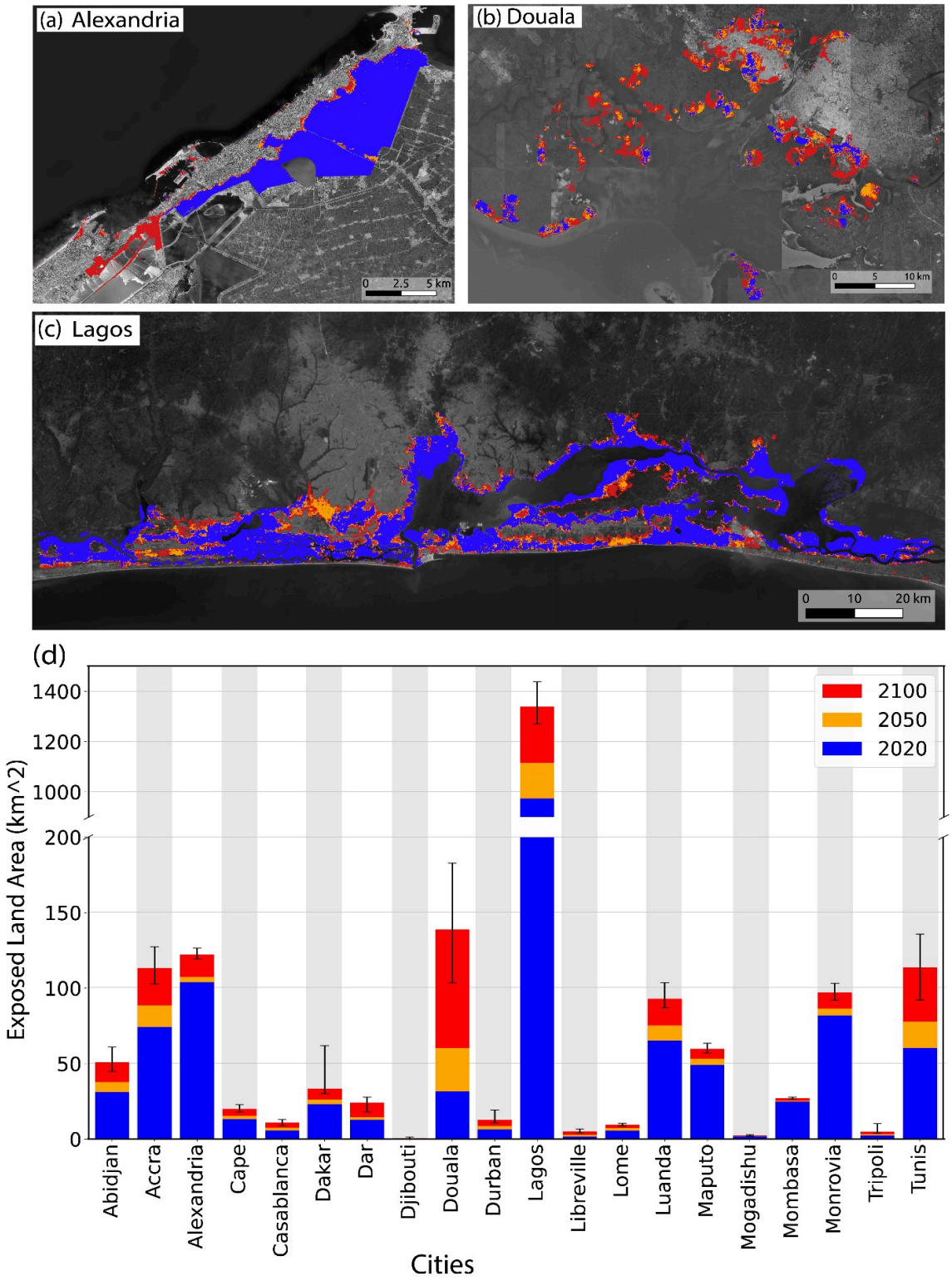


Figure 4

Projected Flood Exposure in Coastal Cities Under Different Sea Level Rise (SLR) Scenarios (a–c) Flood-exposed land in Alexandria, Douala, and Lagos under the SSP 2-4.5 scenario for the years 2020 (blue), 2050 (yellow), and 2100 (red). The progression of inundation highlights the increasing flood exposure over time due to RSL, with substantial land areas in low-lying urban regions projected to be affected by 2100. (d) Projected

exposed land area for each city for the year 2020, 2050 and 2100 under SSP 2-4.5 SLR scenarios. The error bar represents the interquartile range of exposed areas, spanning from the 17th percentile (lower bound) through the median to the upper bound (83rd percentile) for the year 2100.

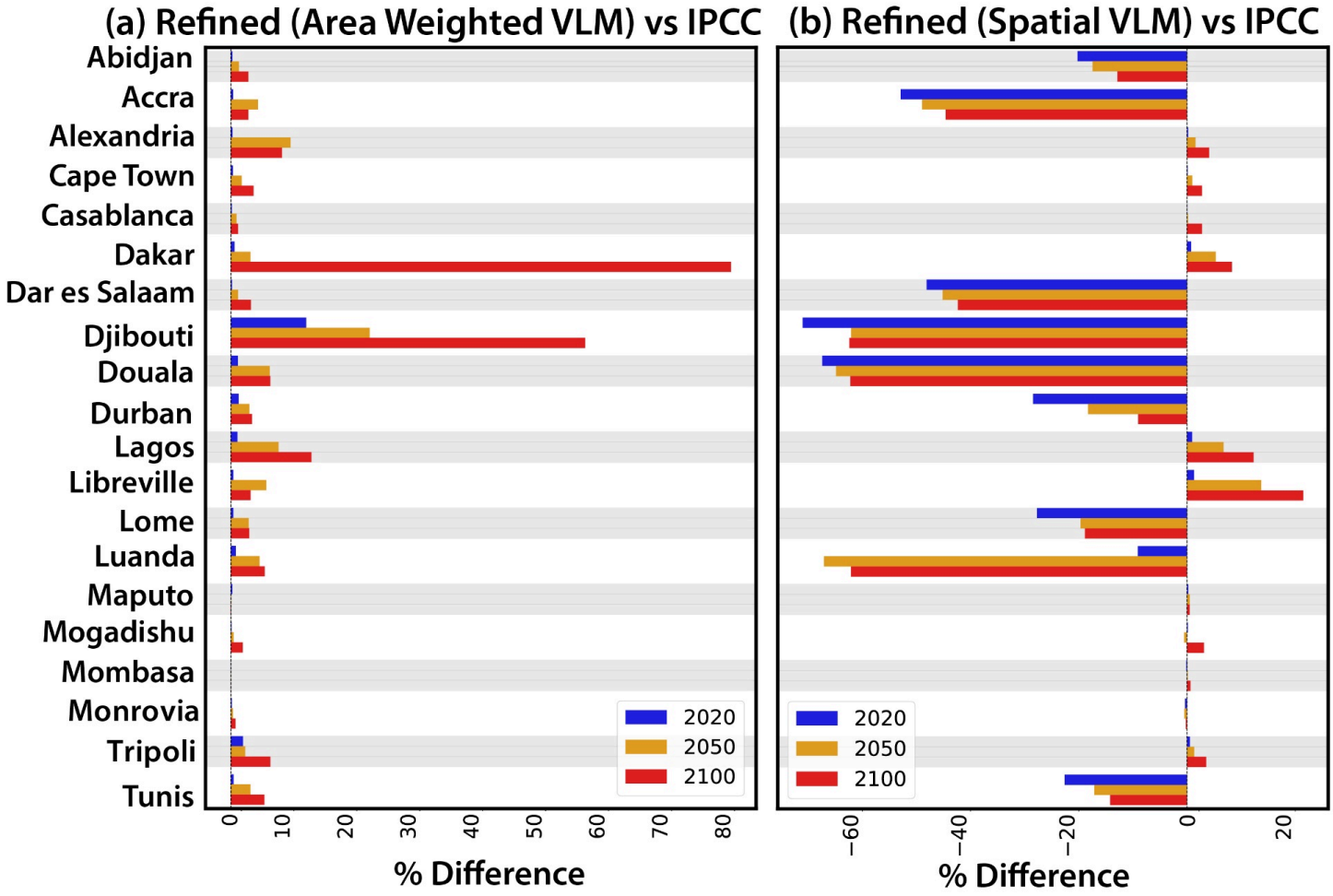


Figure 5

Percentage differences in flood exposure between panels (a) and (b) highlight the impact of spatially varying VLM corrections. (a) Percentage difference in flood exposure between using area-weighted InSAR derived VLM and IPCC projections for each city, showing discrepancies in vertical land motion estimates when spatial variability is not considered. (b) Percentage difference in flood exposure between spatially varied VLM and IPCC VLM projections, capturing finer-scale deviations in vertical land motion across different regions within each city. These differences demonstrate the importance of using localized VLM data for accurate coastal flood risk assessments.

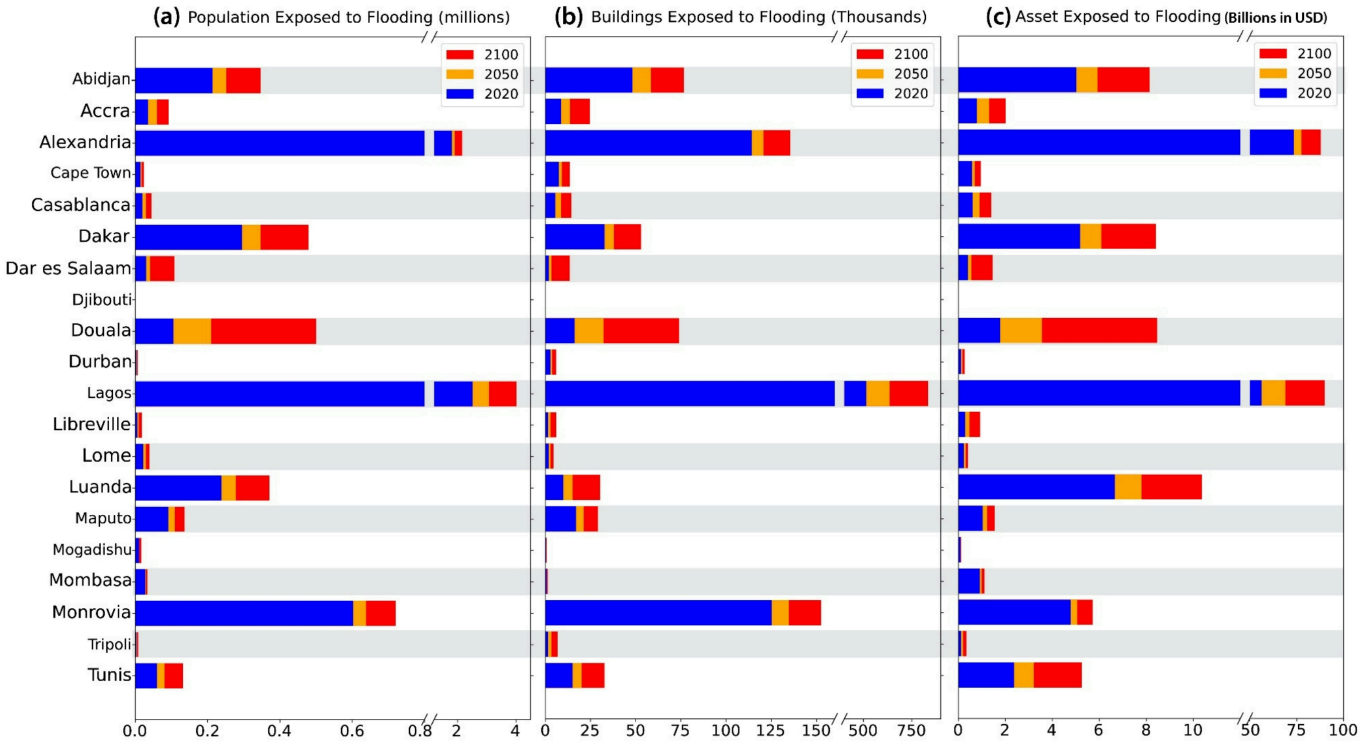


Figure 6

Population, building, and asset exposure to projected flooding for the year 2020, 2050 and 2100. (a) Total population exposed to projected flooding across each of the cities in the study (b) The number of exposed buildings to projected flooding across each city in the study. (c) Cost of exposure to projected flooding in USD (2017 international dollars) based on year 2020 Gross Domestic Product (GDP) per capita.

Supplementary Files

This is a list of supplementary files associated with this preprint. Click to download.

- SupplementaryFile.docx